International Journal of Biological Macromolecules xxx (xxxx) 144181

Contents lists available at ScienceDirect

International Journal of Biological Macromolecules

journal homepage: www.elsevier.com/locate/ijbiomac

Tailoring kraft lignin for high-performance nanoparticles: from structure to function

Jéssica S. Rodrigues [a], Amanda S.M. de Freitas [a], Vagner R. Botaro [b], Marystela Ferreira [b], Leonardo F. Fraceto [a,*]

[a] Institute of Science and Technology, São Paulo State University (UNESP), Av. Três de Março 511, 18087-180 Sorocaba, SP, Brazil
[b] Science and Technology Center for Sustainability (CCTS), Federal University of São Carlos (UFSCar), João Leme dos Santos, km 110, 18052-780 Sorocaba, Brazil

ARTICLE INFO

Keywords:
Sequential fractionation
Acetic acid
Lignin nanoparticles
Functional groups
Nanotechnology

ABSTRACT

In the context of biorefineries, kraft lignin (KL) has emerged as an underexplored yet promising resource. Its phenolic structures are crucial, offering a wide range of applications, from advanced materials to nanotechnology. This study investigates the sequential fractionation of KL in acetic acid (HOAc), a green solvent, to produce lignin nanoparticles (LNP). KL fractions were obtained at HOAc concentrations ranging from 10 % to 60 %. The most promising fractions, namely KL_30%, KL_40%, KL_50%, and the final residue (FR), were selected based on high extraction yield and distinct molar masses (M_w) for LNP preparation using the antisolvent precipitation method. The study explores the influence of M_w, chemical composition, and functionality of LNPs on their properties. The results demonstrated an inverse correlation between M_w and the hydrodynamic diameter of LNPs, where lower M_w fractions (KL_30% and KL_40%) resulted in larger particle sizes, while KL_50%, despite its higher M_w, produced the smallest LNPs. This finding reinforces the idea that M_w alone does not dictate particle size, and the chemical functionality of lignin - particularly the balance between phenolic and aliphatic groups - plays a crucial role in determining aggregation behavior, surface charge, and colloidal stability. A deeper understanding of these structure-function relationships opens new opportunities for optimizing lignin fractionation and tailoring LNPs for specific applications in nanotechnology and advanced materials.

1. Introduction

The circular economy has emerged as a central pillar in the pursuit of more sustainable economic models, aiming to maximize the utilization of natural resources and minimize waste [1]. In the context of biorefineries, this approach has gained prominence by valuing all biomass as a renewable and versatile source. In this scenario, kraft lignin (KL), an abundant and underutilized byproduct of the pulp and paper industry, emerges as a key component [2]. Responsible for 85 % of global KL production, the pulp and paper industry generates approximately 70 million tons of this material annually [3], with projections indicating an increase to 225 million tons by 2030 [4].

During kraft pulping process, lignocellulosic biomass is subjected to an alkaline treatment with an aqueous solution of sodium hydroxide (NaOH) and sodium sulfide (Na_2S) at elevated temperatures and pressures. This process leads to the cleavage of key chemical bonds in lignin, including β-aryl, α-aryl, and α-alkyl ether linkages, resulting in a structurally modified KL with a higher content of phenolic hydroxyl groups. These functional groups enhance KL's reactivity and solubility, making it an attractive candidate for various high-performance applications. The unique structural complexity of KL allows its use in a range of advanced materials, from biofuels and adhesives to nanotechnology and sustainable composites, aligning with the principles of the circular economy and biomass valorization [5,6].

Various fractionation techniques have been widely studied to unlock the full potential of lignin [7]. Sequential fractionation allows for the separation of KL into specific components based on their weight-average molar mass (M_w), offering the opportunity to tailor lignin's properties for nanotechnology applications [8,9]. There are several lignin fractionation methods, each with distinct advantages and disadvantages. For example, acid gradient precipitation is a common method that involves the precipitation of different lignin fractions by gradually decreasing the pH of the solution. While this allows for relatively easy lignin recovery, it can lead to the formation of colloids, resulting in low lignin fraction purity [10–12]. On the other hand, extraction with organic solvents offers high lignin purity but is more complex and energy-

* Corresponding author.
E-mail address: leonardo.fraceto@unesp.br (L.F. Fraceto).

https://doi.org/10.1016/j.ijbiomac.2025.144181
Received 8 January 2025; Received in revised form 5 May 2025; Accepted 11 May 2025
0141-8130/

intensive [13–16]. Ultrafiltration fractionation enables greater control over the molar mass of lignin fractions via membrane cut-off, combined with low cost and energy consumption. However, suffers from limited membrane lifespan due to fouling [17–19].

In many studies, acetic acid (HOAc) has been successfully employed in lignin solubilization during pulping processes, standing out as an effective acidic solvent for extracting this essential biopolymer [20–22]. Additionally, the work by De Oliveira et al. [23] describes a simple and efficient microwave-assisted selective acetylation process of the aliphatic hydroxyl groups of KL promoted by HOAc. Despite its versatility, environmentally friendly properties and effectiveness in solubilization, HOAc has not been explored as a lignin fractionation agent [23]. However, it is important to note that despite its efficacy in solubilization, HOAc has not been explored as a lignin fractionation agent. This gap represents a significant opportunity to investigate the innovative potential of HOAc in producing specific lignin fractions with unique properties. The use of this green solvent for selective lignin fractionation could not only enhance the efficiency of biorefinery processes but also contribute to environmental sustainability, aligning with the principles of the circular economy and offering new perspectives for the comprehensive valorization of lignocellulosic biomass.

Therefore, this study is the first to investigate the effect of sequential fractionation of KL in HOAc to produce tailored lignin nanoparticles (LNP). This study explored the influence of M_w, chemical composition, and functionality on the properties of LNPs. Chemical functionality, especially the presence of phenolic and aliphatic groups, plays a crucial role in influencing the intermolecular interactions and LNP stability. Phenolic groups in lignin primarily include hydroxyl (-OH) groups attached to the aromatic rings of its monomeric units (*p*-hydroxyphenyl, guaiacyl, and syringyl), as well as methoxy (-OCH_3) and, in some cases, carbonyl (C = O) or quinone structures. Aliphatic groups mainly consist of hydroxyl (-OH) groups in the side chains of the phenylpropanoid units, along with minor amounts of carboxyl (-COOH) and aldehyde (-CHO) groups, which may result from oxidation or processing conditions. These functional groups influence LNP properties by affecting their solubility, surface charge, and ability to interact with other molecules. This study contributes to the understanding of the relationship between lignin characteristics and LNP properties, emphasizing the importance of optimizing the fractionation process for applications in nanotechnology and advanced materials.

2. Materials and methods

2.1. Material

Lignin was obtained by the precipitation of black liquor from the industrial process of kraft pulping of *Eucalyptus urograndis* wood. P. A. tetrahydrofuran (THF), acetic acid, and ethyl alcohol were provided by Synth®. Anhydrous citric acid (99.5 %, Êxodo Científica), calcium carbonate, ethanol (99.5 %, Êxodo Científica), gallic acid (GA) (98 %, Êxodo Científica), glacial acetic acid (99.7 %, Êxodo Científica), hydrochloric acid (HCl) (37 %, Neon), methanol (99.8 %, Êxodo Científica), trihydrate sodium acetate (99 %, Êxodo Científica), sodium carbonate (Na_2CO_3) (99.5 %, Êxodo Científica), ferric chloride III hexahydrate ($FeCl_3$) (Êxodo Científica), potassium persulfate ($K_2S_2O_8$) (Êxodo Científica), and sulfuric acid (H_2SO_4) (97.85 %, Neon) were of analytical grade. Folin-Ciocalteu phenol reagent (2 M aqueous solution) was acquired from Êxodo Científica. 2,2-diphenyl-1-picrylhydrazyl (DPPH) was obtained from Sigma-Aldrich. Distilled water was used in all experiments, and the reagents were used as received.

2.2. Sequential fractionation of kraft lignin in acidic medium

KL fractionation was performed, as shown in Fig. 1, in accordance with patent number BR 10 2024 020181 7. The KL used in this study

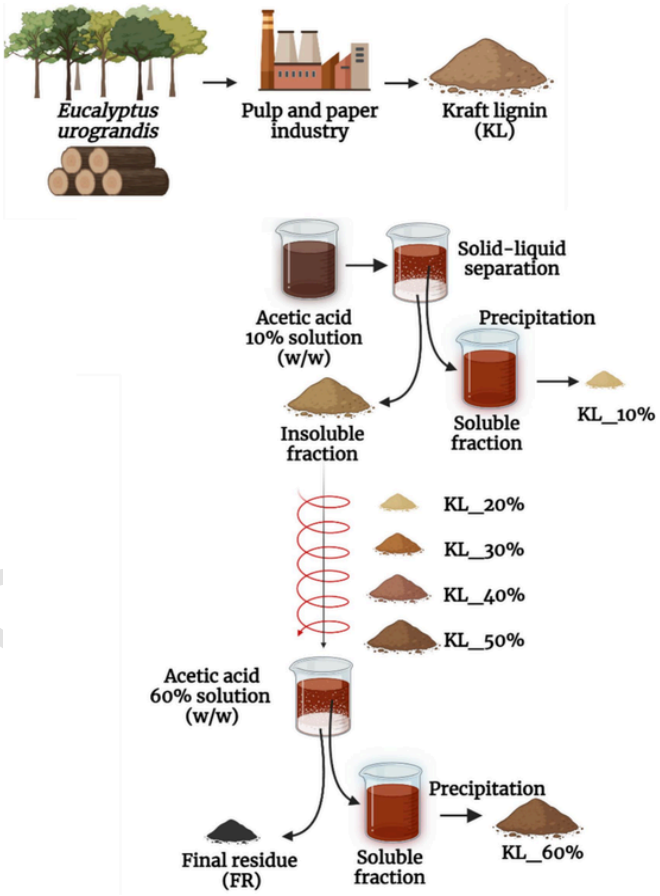

Fig. 1. Illustration of the sequential fractionation approach in an acidic medium. The kraft lignin (KL) from *Eucalyptus urogradis*, derived from the paper and pulp industry, was fractionated into different proportions of acetic acid, followed by the separation of soluble and insoluble fractions. The soluble fraction was precipitated, while the insoluble fraction continued to be fractionated.

was previously characterized in our earlier work [24]. Here, 10 g of KL were added to 100 mL of aqueous solution of HOAc (10 % by volume) and vigorously stirred for 20 min at room temperature (~25 °C). The insoluble lignin (precipitate) was separated by vacuum filtration using qualitative filter paper with a predominant porosity of 18 μm, washed with 100 mL of distilled water to remove excess acetic acid, dried in an oven at 40 °C for 24 h, and subsequently fractionated. The HOAc concentrations used were 10, 20, 30, 40, 50, and 60 %. Approximately 300 mL distilled water was added to the filtrate to precipitate the soluble fraction. Each soluble lignin fraction was named according to the concentrations of KL_10%, KL_20%, KL_30%, KL_40%, KL_50%, and KL_60%, and the final residue (FR). Experimental data were collected in quintuplicate and experimental yields were estimated based on the dry mass of the soluble fractions in HOAc.

2.3. Lignin nanoparticles synthesis

LNP were synthesized using the antisolvent precipitation method, as detailed by Morsali et al. [25]. Initially, previously dried KL (0.5 g) was solubilized in a solution containing 30 g of ethyl alcohol and 10 g of deionized water under constant stirring for 3 h at room temperature. Subsequently, the solution was filtrated through a membrane with 0.45 μm pores (Millipore) to eliminate any undissolved solid material. Finally, to form a colloidal dispersion of KL, 120 g of deionized water

was added to the stirred solution. Ethyl alcohol was then removed through a rotary evaporator, operating under reduced pressure, at 40 °C. The same procedure was performed for the KL_30%, KL_40%, KL_50%, and FR fractions. LNP received the following nomenclature: NPKL, NP30, NP40, NP50, and NPFR, according to the fraction.

2.4. Molar mass determination

The M_w, number-average molar mass (M_n), and polydispersity index (PDI) were determined using Gel Permeation Chromatography (GPC) (Agilent Technologies software model 1260 Infinity II Quaternary System). It was equipped with a refractive index detector (RID), a UV detector (256 nm), and a GPC/SEC pLgel MIXED B column. To construct the calibration curve, polystyrene (PS) standards with a molar mass range of 161–65.7 × 105 g·mol^{-1} (Agilent - Polystyrene High EasiVials 4 mL) were employed. For the analysis, 20 μL of a 1 mg/0.2 mL PS solution in THF was used, with a flow rate of 1 mL.min^{-1}, pressure of 22 bar, and a temperature of 40 °C for the isocratic pump and 40 °C for the RID.

2.4.1. Data analysis

Experimental data were collected in triplicate to report statistically standardized data and compare the experimental efficiencies between M_w at different percentages of the employed HOAc. The significance of the M_w values was analyzed using a one-way analysis of variance (ANOVA) with a 95 % confidence interval ($p = 0.05$). Differences between means were compared and segregated using Tukey's test ($p < 0.05$).

2.5. Characterization methods

2.5.1. Chemical properties and physical structure

2.5.1.1. KL fractions. Structural characterization was conducted using Fourier Transform Infrared Spectroscopy (FTIR) on a Nicolet Summit IR 200 FT-IR instrument in Attenuated Total Reflectance (ATR) mode. Scans were performed at 128.0, with a nominal resolution of 4.0 cm^{-1}, in the range of 4000–400 cm^{-1}. Spectra were acquired using an Ominic Paradigm (Thermo Scientific, USA) and plotted using Origin Pro 8.0. The micromorphologies were observed using Scanning Electron Microscopy (SEM) (TM 3000 Hitachi, Japan) at an acceleration voltage of 15 kV. The samples were coated with gold and palladium using a Denton Vacuum Desk V metalizer (exposure for 90 s, current of 45 mA, and ambient pressure of 0.05 Torr) to ensure proper conductivity. The hydroxyl groups present at different positions in the structure of the KL fractions were determined by ^{31}P Nuclear Magnetic Resonance (NMR) spectroscopy at the National Center for Research in Energy and Materials (CNPEM) in the Bioscience Laboratory (LNBio) in Campinas-SP, following the protocol optimized by Balakshin and Capanema [26]. An Oxford NMR Spectrometer model AS 500. Additional details are included in the supporting information (S1). The Total Phenolic Content (TPC) was determined using the Folin-Ciocalteu colorimetric method, as described by Swain and Hills [27] (Supporting Information, S2). Antioxidant activity was assessed using the 2, 2-diphenyl-1-picrylhydrazyl free radical (DPPH) assay, following the protocol described by Brand-Williams et al. [28] (Supplementary Information – S3).

2.5.1.2. LNP. The size distribution, polydispersity index (PDI), and zeta potential of the LNP were characterized using Dynamic Light Scattering (DLS) with a Malvern Panalytical Zetasizer Ultra. LNP samples were diluted in deionized water (1:1000, *v*/v) before analysis. The stability of the hydrodynamic diameter (nm) of the LNPs was monitored by monthly measurements of the same sample kept at room temperature over a period of four months, using DLS. Morphological characterization of the nanoparticles was performed by Transmission Electron Microscopy (TEM) using a JEOL 2100F model TEM-Bright Field imaging instrument, with spot sizes of 1 nm and a camera length of 10 cm. To determine the Average Size, approximately 50 LNP in the TEM micrographs of each specimen were analyzed using the ImageJ software. The sample was dripped onto a Model C FLATTM grid holder at the National Nanotechnology Laboratory (LNNano). The nanoparticle tracking analysis (NTA) technique was used to determine the nanoparticle concentration and size distribution. A NanoSight LM 10 cell (green laser, 532 nm) with an sCMOS camera and NanoSight software (version 3.1) were used to dilute the nanoparticle suspensions in deionized water (1:10000, *v*/v) before analysis. Five 90-second videos were recorded, shifting the cell content in each video, totaling 1 mL of the diluted sample. Deionized water measurements were conducted to ensure sample integrity and prevent contamination.

2.5.2. Thermal analyses

The thermal characterization of the fractions was carried out using a Perkin Elmer equipment, Pyris1 TGA model, with a constant heating rate of 20 °C.min^{-1} up to 900 °C, maintained in an inert atmosphere with a nitrogen flow rate of 20 mL.min^{-1}. Thermal measurements were conducted using Differential Scanning Calorimetry (DSC) (Q10 model, TA Instruments, USA) equipped with an RCS 40 cooling system. The samples were preheated to 100 °C with 5 min isotherm to eliminate thermal history. Subsequently, the samples were cooled to −10 °C, followed by a second heating to 200 °C with a heating rate of 20 °C.min^{-1}. All measurements were performed under a nitrogen flow of 50 mL/min and the sample mass was maintained at approximately 4–7 mg. Thermal events were identified and calculated during the second heating scan using the TRIOS software.

2.5.3. Solubility of fractions at different pH

To assess the solubility of the lignin fractions, 0.2 g of lignin was added to 10 mL of Na_2HPO_4-citric acid buffer solution (0.1–0.2 M, pH = 4, 6, and 8) or HCl (pH = 2). The mixture was vigorously stirred for 20 min at room temperature and subsequently centrifuged at 12,000 rpm for 10 min to isolate insoluble fractions. The insoluble fraction was then vacuum-filtered and dried in an oven at 40 °C for 24 h. Solubility was determined gravimetrically and expressed as a mass percentage, calculated as the ratio between the dissolved amount and initial mass [29].

3. Results and discussion

3.1. Kraft lignin fractionation in acidic medium

3.1.1. Molar mass distribution

KL from *Eucalyptus urograndis* wood was refined by sequential fractionation using acetic acid (HOAc). In Table 1, it is possible to observe that the extraction yield represents the proportion of lignin solubilized

Table 1
Extraction yield and resulting data from GPC analysis for lignin fractions.

Fraction	Yield (%)	M_w (g·mol^{-1})[a]	M_n (g·mol^{-1})[b]	PDI[c]
KL	–	2653 ± 65	925 ± 37	2.87 ± 0.11
KL_10%	1.91 ± 0.14	710 ± 49*	669 ± 48	1.06 ± 0.14*
KL_20%	7.46 ± 0.57	730 ± 54*	590 ± 10	1.23 ± 0.12*,#
KL_30%	15.17 ± 2.84*	1151 ± 33	892 ± 03	1.29 ± 0.04#
KL_40%	23.67 ± 2.88	1446 ± 70	1093 ± 31	1.33 ± 0.09#
KL_50%	51.06 ± 0.83#	1897 ± 117	1257 ± 90*	1.51 ± 0.06&
KL_60%	50.84 ± 8.64#	2196 ± 99	1416 ± 142*,#	1.55 ± 0.02&
FR	10.89 ± 2.63*	3068 ± 102	1525 ± 58#	2.01 ± 0.15

Symbols Statistically similar samples, in the same column.

[a] M_w, weight-average molar mass.

[b] M_n, number-average molar mass.

[c] PDI, polydispersity index (M_w/M_n).

at each specific percentage of HOAc used. This result was expected because HOAc is widely used in delignification under mild conditions for lignocellulosic materials, a method known as acetosolv pulping [30–32]. As the percentage of HOAc increased, the solubility of lignin in this acidic medium improved, resulting in higher yields of solubilized lignin at higher HOAc concentrations (Table 1). Fractionation did not continue after the addition of 60 % HOAc owing to the low FR percentage.

It is important to note that the extraction yields presented in Table 1 refer to each fraction obtained sequentially from the insoluble residue of the previous step. Therefore, yields were calculated individually at each stage based on the lignin mass recovered after precipitation, not cumulatively from the initial KL mass. As a result, the sum of all fractions (KL_10% to KL_60% and FR) may exceed 100 %. This is not a mass balance inconsistency but a reflection of the independent yield calculation used in the cascade fractionation process.

The M_w, M_n, and PDI of each fraction are presented in Table 1 and correlated in Fig. 2. The fractions M_w increased gradually from KL_10% (710 g.mol^{-1}) to KL_60% (2196 g.mol^{-1}). This result indicates that low molar mass fractions were predominantly solubilized at lower percentages of HOAc (KL_10%, KL_20%, and KL_30%), whereas higher molar mass fractions were solubilized at higher acid concentrations (KL_50% and KL_60%). The PDI of the fractions increased as fractionation proceeded, with KL and FR showing higher PDI values than those of the other fractions (Fig. 2).

Statistical analysis was performed using a one-way ANOVA, and the results are shown in Fig. 2. The calculated *p*-value was <0.05, indicating a statistically significant difference between the analyzed compositions. Therefore, it was necessary to conduct a Tukey's test between the two samples, assuming different variances. Pairwise analysis of the compositions revealed that only the sample sets KL_10% and KL_20% (a), KL_50% and KL_60% (b), and KL_60% and KL (c) showed no significant differences in their M_w values. The other analyzed combinations exhibited differences within their sets. Thus, KL was separated into specific fractions with low, medium, and high ranges of M_w.

The fractions for the subsequent steps were carefully selected considering the yield efficiency percentage and statistical discrepancies between sample sets. The KL_10% and KL_20% fractions were omitted in the subsequent steps because of their low yield efficiency (Table 1), while the KL_60% sample was excluded because of its similarity to the KL_50% and KL samples (Fig. 2).

3.2. Chemical properties and physical structure

Fig. 3 shows photographic images of the four fractions obtained, showing noticeable color variations among the samples. A darkening trend was observed from KL_30% (Fig. 3B) to FR (Fig. 3E), indicating potential discrepancies in the chemical structures of the fractions. In addition, the gradual darkening of the samples was proportional to the increase in M_w (Table 1). Therefore, detailed analyses were conducted to investigate the trends in the molar mass, chemical functionality, solubility, and thermal properties of the lignin fractions.

SEM was used to examine the micromorphologies of the different KL fractions (Fig. S3). SEM micrographs of the KL_30%, KL_40%, and KL_50% fractions (Fig. 3B–D) resembled KL (Fig. S3A), indicating that these fractions were processed and isolated such that the morphological structure of lignin remained practically unchanged. Micrographs of KL, KL_30%, KL_40%, and KL_50% were captured at the same magnification (x800), whereas the FR fraction was enlarged to x80 due to its particles were 10 times larger. Notably, the reduced magnification of the FR fraction micrograph suggests an excess of HOAc. This excess could result from more severe solubilization conditions, affecting the integrity of the lignin structure and causing morphological and chemical alterations.

The FTIR spectra of the four lignin fractions, along with KL, displayed characteristic lignin absorption bands (Fig. 3F), including OH stretching at 3400 cm^{-1}, CH stretching between 2836 and 2939 cm^{-1}, and aromatic skeletal vibrations at 1602, 1511, 1456, and 1419 cm^{-1}. Additionally, CO stretching was observed at 1212 cm^{-1}, and aromatic in-plane CH deformation at 1032 cm^{-1}. These functional groups mainly originated from guaiacyl and syringyl units, consistent with lignin extracted from *Eucalyptus urograndis* [15]. A weak signal at 1709 cm^{-1} indicated a low carboxyl content, while the strong peak at 1212 cm^{-1} suggested a predominance of phenolic units over carboxyl groups [24]. Although FTIR did not reveal significant structural changes, complementary techniques such as NMR and phenolic content analysis were

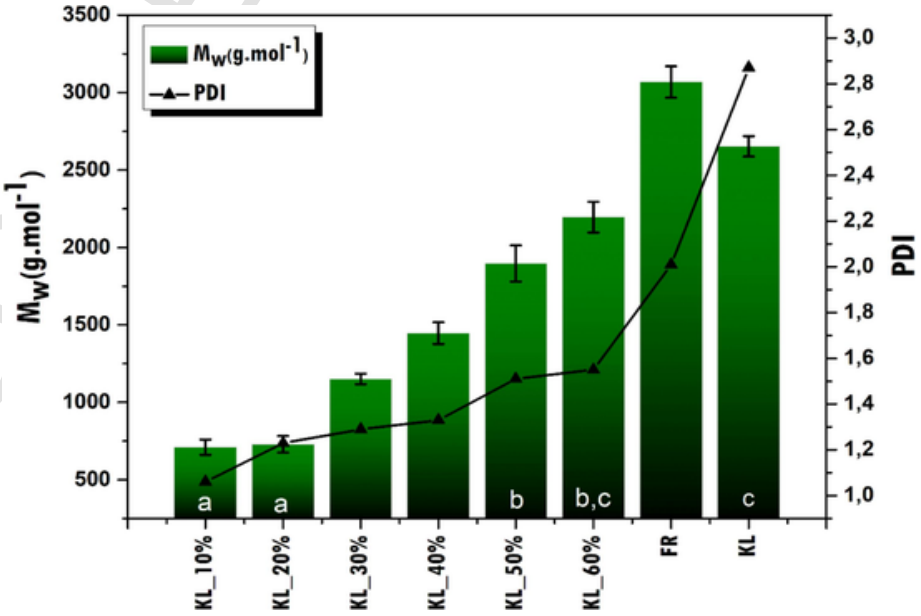

Fig. 2. Correlation between weight-average molar mass (M_w) and polydispersity index (PDI) of fractions: KL_10%, KL_20%, KL_30%, KL_40%, KL_50%, KL_60%, FR, and KL. [a–c] Statistically similar samples.

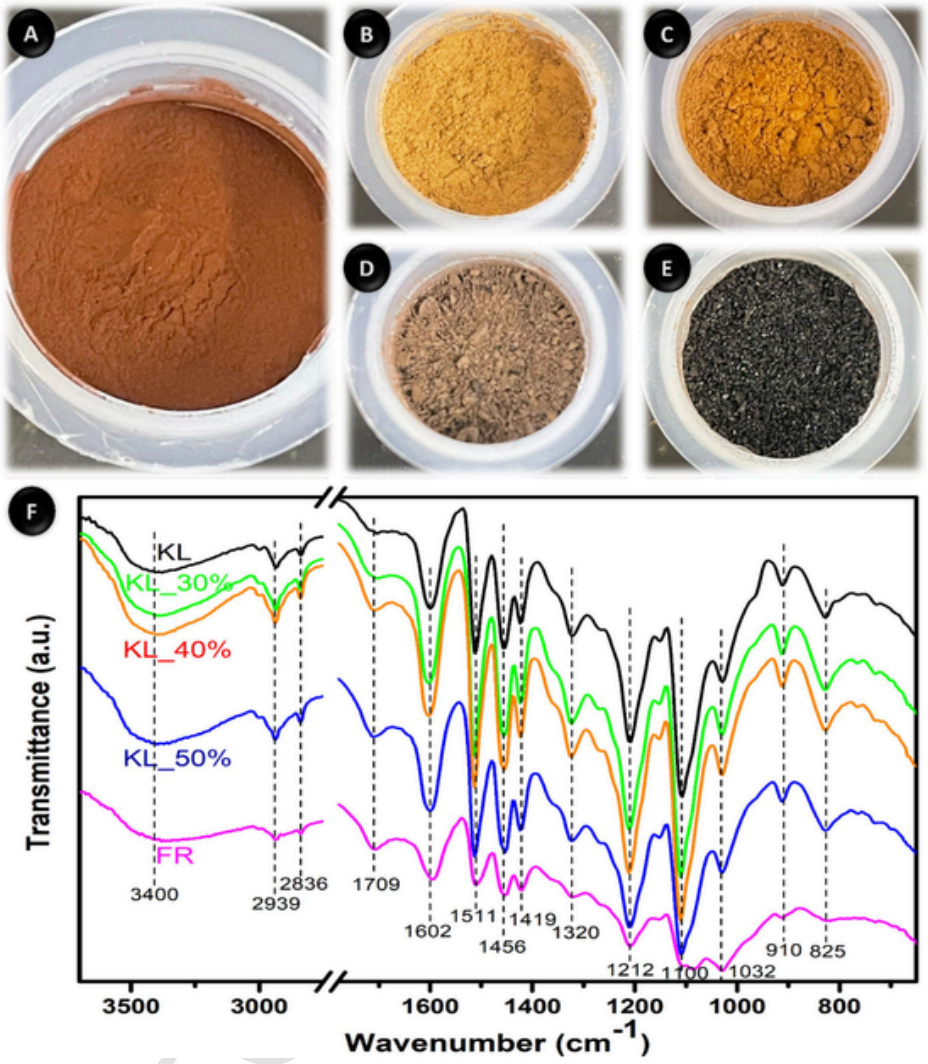

Fig. 3. Sample photographs: KL (A), KL_30% (B), KL_40% (C), KL_50% (D), and FR (E). These samples were obtained through sequential fractionation in acetic acid, with emphasis on the darkening of the samples as the percentage of acid increased. (F) FTIR spectra of the KL sample (black), KL_30% (green), KL_40% (red), KL_50% (blue), and FR (pink). (For interpretation of the references to color in this figure legend, the reader is referred to the web version of this article.)

employed to gain a more comprehensive understanding of the modifications induced by fractionation. Each technique provided distinct insights, ensuring a thorough characterization of the lignin fractions.

3.2.1. Content of phenolic hydroxyl groups vs. solubility

The ^{31}P NMR analysis of lignin enabled the quantification of various types of hydroxyl groups, including aliphatic and phenolic groups and carboxyl groups, as shown in Table 2 and Fig. S4 [26]. The KL_30% fraction exhibited a higher content of phenolic hydroxyl groups (3.47 mmol.g^{-1}), while the KL and FR fractions showed higher amounts of aliphatic hydroxyl groups, recording 1.55 and 1.54 mmol.g^{-1}, respectively. Furthermore, because of the fractionation process used, the phenolic units S and G increased gradually in the KL_30% fraction (2.73 mmol.g^{-1}) compared with the other fractions (2.25, 1.95 and 1.05 mmol.g^{-1}) leading to an increase in the number of theoretical reactive sites.

Therefore, the Ph-OH content gradually increased as the M_w of the fractions decreased, whereas Alf-OH and COOH showed an inverse trend. The TPC values of the lignin fractions ranged from 35.36 ± 3.76 to 65.52 ± 2.65 μg.GAE/mg, as shown in Table 2. KL_30% had the highest total phenolic content (65.52 μg.GAE/mg), while FR had the

Table 2
Analysis of KL, KL_30%, KL_40%, KL_50%, and FR by ^{31}P NMR and Total Phenolic Content (TPC).

Fraction	Aliph-OH	5-sub	G_{nc}	H	Total Ph-OH	Total OH	COOH	TPC
	mmol/g							(μg·GAE/mg)
KL	1.55	2.57	0.44	0.24	3.25	4.80	0.48	46.65 ± 3.20[a]
KL_30%	1.35	2.73	0.50	0.24	3.47	4.82	0.63	65.52 ± 2.65
KL_40%	1.46	2.25	0.36	0.21	2.81	4.27	0.77	53.60 ± 2.68
KL_50%	1.49	1.95	0.33	0.23	2.50	3.99	0.76	46.99 ± 3.69[a]
FR	1.54	1.05	0.33	0.41	1.79	3.33	1.50	35.36 ± 3.76

Alif-OH = aliphatic hydroxyl; 5-sub = 5-Substituted Phenols (Condensed Syringyl and Guaiacyl); Gnc = non-condensed guaiacyl; total Fen-OH = total phenolic hydroxyl; total OH = total hydroxyl groups; COOH – Carboxyl Groups; TPC - Total Phenolic Content; GAE = Gallic Acid Equivalent. [a] Statistically similar samples.

lowest phenolic content (35.63 μg.GAE/mg), corroborating the ^{31}P NMR results. Additionally, the KL and KL_50% samples showed no significant differences in TPC. These results indicate that the Ph-OH groups were easily solubilized at low percentages of HOAc.

The evident increase in Ph-OH groups indicated enhanced solubilization in lower M_w fractions due to substantial cleavage of β-O-4 linkages, leading to an abundance of terminal groups. This aligns with findings from studies on KL fractionation, emphasizing the increase in Ph-OH groups and concurrent reduction in Aliph-OH groups with decreasing lignin M_w [14,33–35]. The significant increase in COOH groups in the FR was attributed to more intense reactions and the breaking of chemical bonds resulting from more rigorous process conditions due to the high concentration of HOAc. Although KL and KL_30% exhibit similar total hydroxyl content (4.80 and 4.82 mmol·g^{-1}, respectively), their internal composition differs significantly. KL_30% is enriched in Ph-OH, especially syringyl and guaiacyl units, whereas the parent KL has a more balanced profile, with a higher proportion of Aliph-OH groups. In contrast, the KL_40%, KL_50%, and FR fractions showed a progressive reduction in total OH content, despite representing a larger mass proportion of the original lignin. This trend can be attributed to the increasing M_w and structural condensation of these fractions, which reduces the number of terminal and reactive hydroxyl groups accessible for phosphitylation during ^{31}P NMR analysis. Therefore, the similarity in total OH between KL and KL_30% does not indicate similar chemical reactivity or structure but reflects different distributions of functional groups within each sample.

Subsequently, the investigation of the solubility of the lignin fractions in Na_2HPO_4 -citric acid buffer at pH levels ranging from 2 to 8 further complemented the understanding of their chemical characteristics. As illustrated in Fig. S5, a consistent increase in solubility was noted across all fractions with increasing pH. Particularly noteworthy was the Enhanced solubility was observed in fractions rich in Ph-OH groups (Solubility > KL_30% > KL > KL_40% > KL_50 > FR). This observation suggests a direct association between the presence of Ph-OH groups and increased solubility, especially under alkaline conditions, attributed to their capacity to form hydrogen bonds and foster more favorable interactions [36,37].

3.2.2. Thermal properties

The results of Thermogravimetric Analysis (TGA) and Derivative Thermogravimetry (DTG) curves (Fig. 4) are presented in Table 3. The analyzed parameters included $T_{5\%}$ (onset temperature of degradation with a 5 % mass loss), T_{max} (temperature at the maximum mass loss rate), Δm (mass loss rate until Tmax), and $R_{900°C}$ (carbonaceous residue at 900 °C).

In a general overview, the small, broad peaks preceding the main event observed in the DTG curves (Fig. 4B) in the region of 100 °C to 150 °C were related to the removal of residual moisture adsorbed on the sample surfaces [38]. An early $T_{5\%}$ was observed for the KL_40% sample, indicating a higher moisture percentage in this sample. Losses between 150 and 300 °C were attributed in the literature to the presence of residual carbohydrates with lower molar mass from lignin [39,40]. In the range of 350–450 °C, the thermal degradation event showed a close Δ_m range among the fractions (KL, KL_30%, KL_40%, and KL_50%), with this temperature range being characteristic of the thermal degradation of low molar mass and polyphenolic nature units [41,42].

It was observed that the $R_{900°C}$ of the lignin fractions increased proportionally to the M_w (Table 1), indicating a correlation with the higher branching and condensation of FR, KL_50%, and KL compared to KL_40% and KL_30%. According to a previous study, lignin with higher M_w presents a higher yield of $R_{900°C}$; however, as the content of functional groups (hydroxyl and methoxyl) increases, the char residue decreases [14]. This study highlighted this phenomenon, where KL, with a higher M_w (2653 g.mol^{-1}), exhibited a lower $R_{900°C}$ than the KL_50% fraction. This observation is supported by the hypothesis that there is a higher percentage of low M_w lignin in KL, given that this fraction was not subjected to fractionation. In other words, the thermal degradation behavior of the fractions was directly correlated with the active functional groups, as high M_w fractions require more thermal energy to break the β-O-4 linkages present in their structure. In contrast, in the lower M_w fraction, such linkages were less abundant [19,].

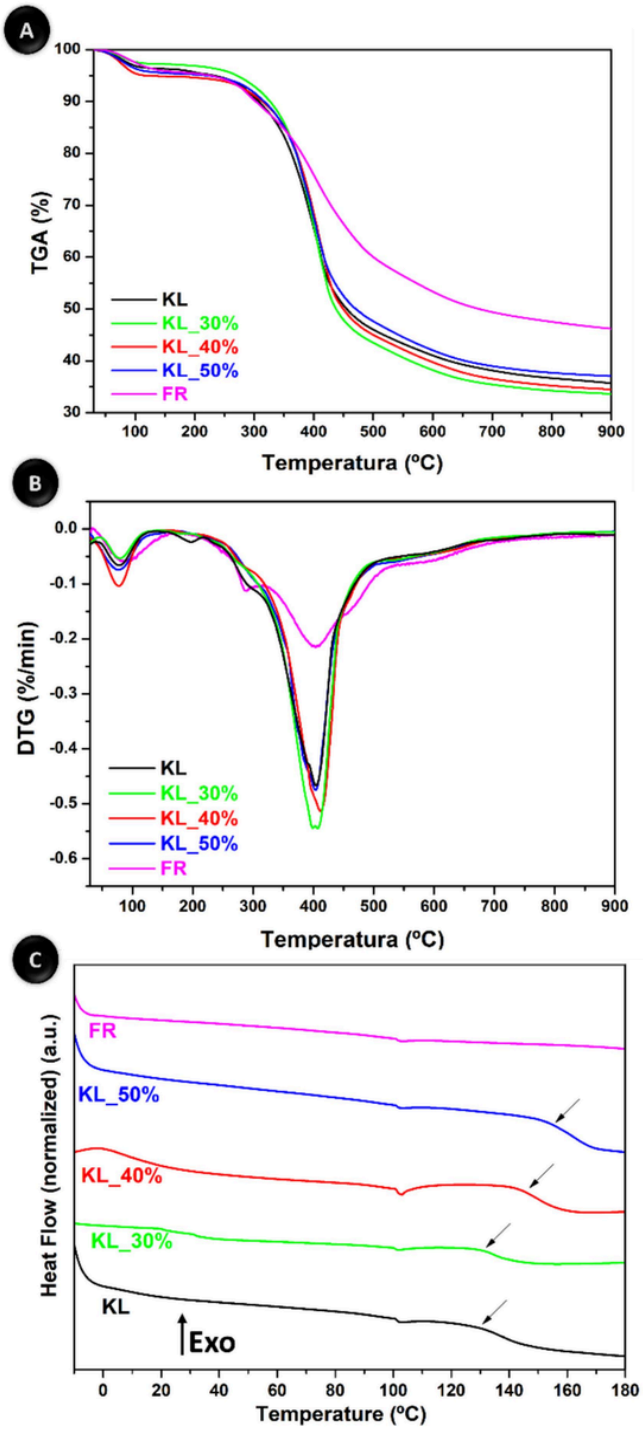

Fig. 4. (A) Thermogravimetric Curves (TG), (B) First Derivative of Thermogravimetric Curves (DTG), and (C) Differential Scanning Calorimetry (DSC) for the lignin fractions: KL, KL_30%, KL_40%, KL_50%, and FR.

Table 3
Results of thermogravimetric analyses for the KL fractions.

Fraction	$T_{5\%}$(°C)[a]	T_{max}(°C)[b]	Δ_m(%)[c]	$R_{900°C}$(%)[d]
KL	232	405	37	35
KL_30%	268	403	36	33
KL_40%	116	412	38	34
KL_50%	218	403	34	37
FR	226	405	25	46

[a] Onset temperature of degradation;
[b] Temperature at the maximum mass loss rate.
[c] Mass loss rate until T_{max};
[d] Carbonaceous residue at the end of the degradation process.

DSC analysis was conducted to determine the glass transition temperatures (T_g) of the lignin fractions (Fig. 4C). The DSC curves revealed that the KL and KL_30% fractions exhibited the lowest T_g values, below 130 °C, while the KL_40% and KL_50% fractions showed higher values, around 140 and 150 °C, respectively. Previous studies indicated that a low M_w resulted in an increase in the free volume of the polymer, consequently leading to a decrease in T_g [14]. This behavior was observed in the KL_30%, KL_40%, and KL_50% fractions, where the increase in M_w was proportional to the increase in the T_g value. However, the KL fraction did not follow this pattern due to the complexity of its heterogeneous structure. It was not possible to determine the T_g value of FR, which was associated with its high thermal stability, as evidenced by the TGA data.

3.2.3. Antioxidant activity

The antioxidant properties of lignin are primarily linked to the ability of its phenolic structures to scavenge ROS-containing free radicals. To understand the effect of fractionation on the antioxidant properties of the lignin fractions, free-radical scavenging analyses were conducted using the DPPH method, as shown in Table 4. This process involves the formation of a stable non-radical DPPH-H complex through a reaction between DPPH and proton-donating substrates [44] with IC_{50} values indicating the concentration that inhibits 50 % of the initial DPPH radicals. The results showed that the KL_30% fraction was the most effective scavenger of free radicals against DPPH, whereas FR had the lowest antioxidant activity. Additionally, minimal concentrations of KL_30% (6.8 %) were sufficient to achieve IC_{50}, which was also observed for EC_{50}.

As reported in previous studies [44–46], a higher concentration of hydroxyl and methoxy phenolic groups is directly associated with increased antioxidant activity, because these groups have the ability to stabilize phenoxy radicals. These phenolic groups donate electrons to the free radicals, thereby neutralizing their harmful effects. Specifically, the additional stabilization provided by the hydroxyl phenolic groups at the ortho position is noteworthy. These groups act through resonance, redistribute electrons between bonds, and provide greater stability to phenoxy radicals. These factors prevailed over the influence of M_w and polydispersity [46]. These is consistent with the results of this study, in which the KL_30% fraction demonstrated notable efficacy in eliminating free radicals against DPPH, indicating a positive correlation with the presence of hydroxyl phenolic groups. The observation that minimal concentrations of KL_30% were sufficient to achieve IC_{50} reinforces the association between low M_w, high TPC, and antioxidant efficacy.

Table 4
Antioxidant activity data using the 1,1-diphenyl-2-picrylhydrazyl (DPPH) radical method.

Fraction	DPPH		
	Reduction %	IC_{50} (mg/L)	EC_{50} (mg lig/mg)
KL	67.98 ± 3.65[a]	8.6 ± 0.69[a,b]	0.72 ± 0.08
KL_30%	76.32 ± 2.43	6.8 ± 0.32	0.57 ± 0.03
KL_40%	62.72 ± 2.69[a]	8.1 ± 0.78[a]	0.68 ± 0.02
KL_50%	63.60 ± 3.58[a]	9.5 ± 0.75[b]	0.79 ± 0.06
FR	48.25 ± 2.41	12.6 ± 0.83	1.05 ± 0.08

IC_{50} - half-maximal inhibitory concentration; EC_{50} - Half-maximal effective concentration.
[a] Statistically similar samples.

3.3. Lignin nanoparticles (LNP) characterization

TEM was used to evaluate the morphology of the prepared LNP, as shown in Fig. 5. The microscopic images revealed that the sample derived from KL (NPKL) contained nanoparticles with diverse contours and sizes. When compared to the LNPs prepared from fractions (NP30, NP40, and NP50), larger particles were observed. The NP30 sample derived from KL_30% showed the most promising results, displaying a repetitive spherical pattern with well-defined contours and more uniform particle sizes, as previously reported [47,48]. NP40 and NP50 also presented superior results compared with NPKL, showing a spherical and homogeneous morphology. However, the NPFR sample yielded less satisfactory results, with particles characterized by irregular contours and the absence of a morphological pattern.

After a systematic evaluation using the ImageJ software to determine the average size of the nanoparticles in the TEM micrographs, it was concluded that the LNP had an average size of approximately 70–126 nm (Table 5). The hydrodynamic particle diameter data presented in Table 5 corroborate the observations from the TEM micrographs. The NPKL sample exhibited the highest average hydrodynamic diameter, measuring 251 ± 9 nm. For the nanoparticles derived from the fractionated samples (NP30, NP40, and NP50), the average values were 128 ± 3, 117 ± 2, and 106 ± 2 nm, respectively, indicating a close range of diameters. The hydrodynamic diameter decreases as the percentage of HOAc increases during fractionation. Previous studies in the literature have also reported nanoparticles with diameters below 200 nm after solvent fractionation of kraft lignin from hardwood and softwood [48]. The NPFR sample showed the smallest diameter value (63.2 nm). However, this result was not interpreted positively because TEM micrographs were required to reveal adequate dispersion and homogeneity in terms of size and contour. Additionally, the low solubility of this sample was observed throughout all procedures.

The PDI results (Table 5) confirmed the TEM results. The NP30, NP40, and NP50 samples, which exhibited similar morphologies and hydrodynamic diameters, also exhibited similar PDI values, ranging from 0.08 to 0.13. In the literature, a PDI between 0.0 and 0.1 is considered ideal for LNP. Elevated values have been associated with a low effective concentration of lignin polymer, reducing the ability to interact and form nanostructures [48]. On the other hand, the NPFR sample, with a PDI of 0.503, indicated that the formation and stability of LNP were not efficient for this sample.

In the zeta potential analysis (Table 5), all samples exhibited values close to or negative, ranging between −25 and −31 mV. Similar values have been previously reported in the literature (−14 to −31 mV) [47]. It is common for LNP to maintain negative zeta potential values because of the negative charge of phenols and, to some extent, the adsorption of hydroxide ions [49,50]. These data on the surface charges of LNP can provide relevant information about stability. When the suspended particles have similar zeta potentials, repulsion tends to occur, indicating a low propensity for agglomeration. Therefore, particles with zeta potentials more positive than +30 mV or more negative than −30 mV are considered stable [51]. The results indicated adequate solution stability for the NPL produced in this study [52].

The assumption that LNPs would remain stable over time, based on their initial physicochemical properties (zeta potential and size distribution), was tested through hydrodynamic diameter analysis over four months, as shown in Fig. S6. During this monitoring period, all samples

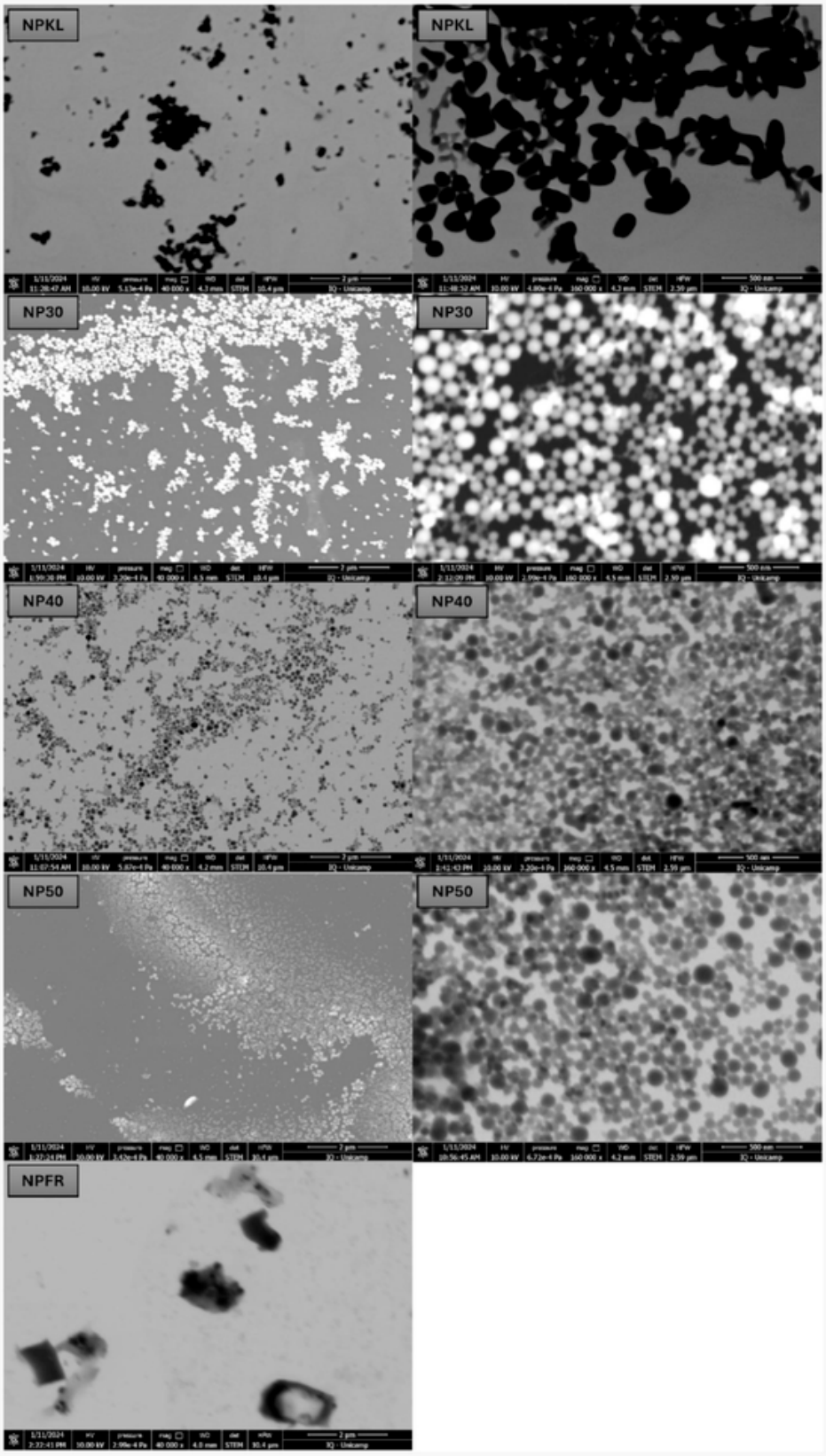

Fig. 5. TEM micrographs obtained for the samples NPKL, NP30, NP40, NP50, and NPFR at magnifications of 40,000× (left column) and 160,000× (right column).

Table 5
Data of hydrodynamic diameter (nm), Zeta potential (mV), and PDI obtained by DLS, size distribution (nm) by NTA, and average size (nm) by TEM for the samples: NPKL, NP30, NP40, NP50, and NPFR.

	DLS			NTA		TEM
	Hydrodynamic diameter (nm)	PDI*	Zeta potential (mV)	Hydrodynamic diameter (nm)	Concentration (Particles/mL)	Average size (nm)
NPKL	251 ± 9	0.251 ± 0.03	−30.9 ± 0.7[a]	230 ± 9	$9.7 \times 10^{12} \pm 6.5 \times 10^{11}$	126.77 ± 29[a]
NP30	128 ± 3	0.120 ± 0.02[a]	−27.4 ± 0.8[b]	146 ± 8[a]	$1.6 \times 10^{13} \pm 5.5 \times 10^{11}$	100.57 ± 10[a]
NP40	117 ± 2	0.080 ± 0.01	−30.6 ± 0.7[a]	139 ± 3[a,b]	$2.6 \times 10^{13} \pm 2.1 \times 10^{12a}$	72.83 ± 12[b]
NP50	106 ± 2	0.130 ± 0.03[a]	−25.9 ± 0.9	134 ± 2[b]	$2.2 \times 10^{13} \pm 1.1 \times 10^{12a}$	70.04 ± 14[b]
NPFR	63 ± 1	0.503 ± 0.09	−25.0 ± 3.0[b]	99 ± 6	$1.7 \times 10^{12} \pm 8.4 \times 10^{11}$	–

[a,b]Statistically similar samples, for the same column.
* PDI. polydispersity index.

maintained stable diameters except for the NPKL sample, which showed a slight reduction in diameter in the last month. The hydrodynamic diameter was measured using DLS, which provides an ensemble-averaged size distribution and is highly sensitive to larger particles. While DLS was used to assess stability, NTA could complement these results by offering number-weighted size distributions and detecting subpopulations of nanoparticles.

The synthesized nanoparticles were also analyzed by Nanoparticle Tracking Analysis (NTA). This technique uses the properties of light dispersion and Brownian motion to obtain the hydrodynamic diameter of nanoparticles in liquid suspension [44]. The results in Table 5 show that the hydrodynamic volume obtained by NTA follows the same pattern as the hydrodynamic volume obtained by DLS [53]. The values increase as the M_w of the fractions decreases, following the order NP50 > NP40 > NP30. The difficulty in performing NTA on the NPFR sample was correlated with the high irregularity of the particles, as observed in the TEM micrographs. The hydrodynamic volumes obtained by NTA and DLS may differ owing to variations in the measurement techniques. Whereas DLS provides a weighted average of particle sizes, NTA tracks individual movements by considering each particle. Discrepancies are common because of experimental variations and the specific sensitivities of the methods. It was also possible to measure the particle concentration per milliliter using NTA. The NPKL and NPFR samples exhibited the lowest concentrations, while the others (NP30, NP40, and NP50) maintained similar concentrations.

3.4. M_w and chemical composition vs. LNP size

As previously outlined in research, the formation of LNP is driven by π-π interactions and hydrogen bonding between the phenolic rings of lignin [54–56]. Additionally, the number of phenolic and aliphatic units has a direct impact on the LNP hydrodynamic diameter [48]. Fig. 6 established a correlation between M_w and the chemical functionality of lignin fractions, illustrating how these factors influence the hydrodynamic volume of produced LNP. A decrease in the hydrodynamic diameter of the LNPs was observed as M_w increased. Fractions with a lower M_w, such as KL_30% and KL_40%, resulted in larger sizes (128 and 117 nm, respectively), whereas the KL_50% fraction, with a higher M_w, exhibited a smaller diameter of 106 nm.

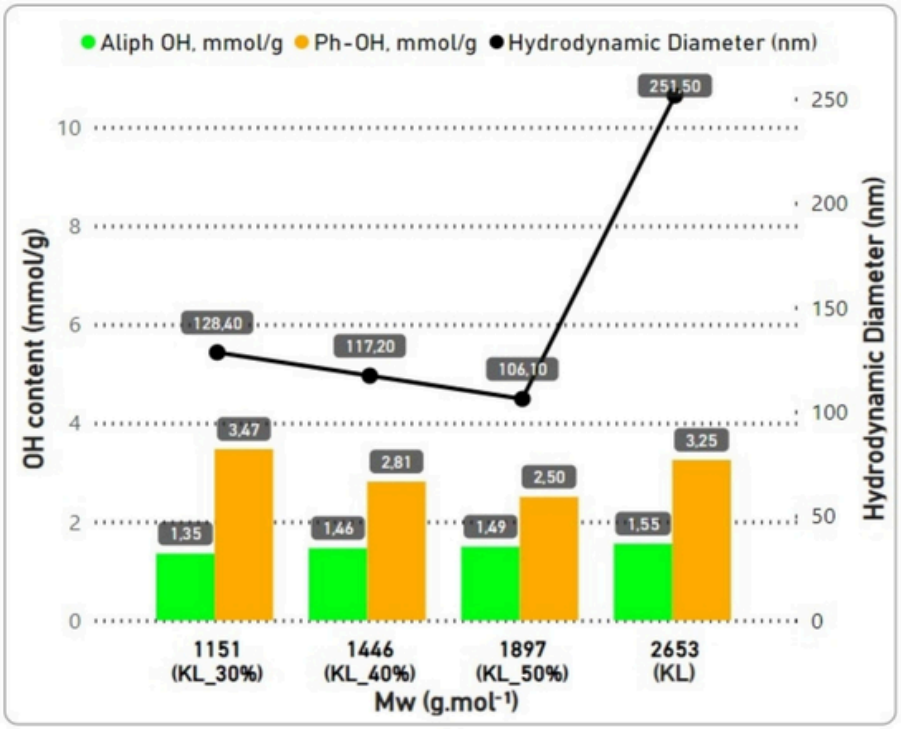

Fig. 6. LNP hydrodynamic diameter as a function of M_w and the contents of Ph-OH and Aliph-OH.

The relationship between LNP size and the number of Ph-OH and Aliph-OH groups in the lignin fractions was also identified. The LNP hydrodynamic diameter decreased with a reduction in the number of Ph-OH units and an increase in the number of Aliph-OH units in the lignin fractions. A higher number of Ph-OH favored interaction between lignin molecules, resulting in stronger hydrogen bonding and π-π stacking, leading to the formation of larger LNP [55]. On the other hand, an increase in Aliph-OH reduced the ability of lignin molecules to establish non-covalent bonds with other lignin molecules, restricting LNP size and resulting in smaller particles [54].

The structural characteristics of lignin fractions, particularly the M_w distribution and functional group composition, significantly influenced the formation and stability of LNPs. Lower M_w fractions (KL_30% and KL_40%) exhibited a greater number of Ph-OH groups, leading to enhanced π-π interactions and hydrogen bonding, which facilitated the formation of larger LNPs. Conversely, KL_50%, despite its higher M_w, resulted in smaller LNPs, suggesting that Aliph-OH contributed to reducing intermolecular interactions and limiting particle growth. This observation reinforces the idea that the balance between Ph-OH and Aliph-OH functionalities governs the colloidal behavior of LNPs, affecting their surface charge (zeta potential), solubility, and aggregation tendency.

Beyond their physicochemical properties, these structural attributes dictate the potential of LNPs in targeted applications. Recent studies have demonstrated that LNPs can be utilized in controlled release systems, where their stability and tunable size influence the diffusion of active compounds [57]. Additionally, the strong π-π interactions and the presence of phenolic groups make LNPs attractive for antioxidant and UV-protective coatings, offering potential applications in sustainable packaging and functional surfaces [58]. Moreover, LNPs have been reported as effective stabilizers in Pickering emulsions, particularly for food and cosmetic formulations, leveraging their amphiphilic nature [59]. Their potential integration into biodegradable polymer nanocomposites has also been explored, where they can enhance mechanical properties and thermal stability [60].

Understanding this intricate structure-function relationship is crucial for designing lignin-derived nanoparticles with tailored physicochemical properties, optimizing their performance across different technological applications. Further research could explore how fine-tuning lignin fractionation parameters can enhance the applicability of LNPs in these and other emerging fields.

4. Conclusion

This study provides valuable insights into lignin nanotechnology by demonstrating how sequential fractionation of KL in HOAc influences LNP synthesis. The KL_30%, KL_40%, KL_50%, and FR fractions emerged as the most relevant for LNP production, with a clear inverse correlation between M_w and hydrodynamic diameter. While higher M_w is often expected to lead to larger particles, our results indicate that chemical composition plays an equally significant role, particularly the balance between Ph-OH and Aliph-OH groups. KL_50%, despite having the highest M_w among the tested fractions, produced the smallest LNPs, confirming that a reduction in Ph-OH content and an increase in Aliph-OH groups contributed to smaller particle sizes. These findings enhance our understanding of the relationship between lignin characteristics and LNP properties, opening new opportunities for practical applications. The optimized LNPs developed in this study hold significant potential in nanotechnology and advanced materials, including encapsulation and controlled release systems for agrochemicals and pharmaceuticals, UV-protective and antioxidant coatings for packaging and smart materials, antimicrobial wound dressings, stabilizers in Pickering emulsions for cosmetics and food formulations, and bio-based adhesives and composites for sustainable construction and automotive industries. This study highlights the importance of an integrated approach to LNP design, considering both M_w and chemical composition, to drive innovative applications. Furthermore, these results provide a foundation for scaling up lignin-based nanoparticle production for industrial applications, contributing to the development of sustainable nanomaterials on a larger scale.

CRediT authorship contribution statement

Jéssica S. Rodrigues: Writing – original draft, Validation, Methodology, Investigation, Formal analysis, Data curation, Conceptualization. **Amanda S.M. de Freitas:** Writing – original draft, Formal analysis, Data curation, Conceptualization. **Vagner R. Botaro:** Writing – review & editing, Conceptualization. **Marystela Ferreira:** Writing – review & editing, Supervision, Resources. **Leonardo F. Fraceto:** Writing – review & editing, Visualization, Supervision, Resources, Project administration, Investigation, Funding acquisition, Conceptualization.

Declaration of competing interest

The authors declare that they have no known competing financial interests or personal relationships that could have appeared to influence the work reported in this paper.

Acknowledgements

This research was partially funded by the State of São Paulo Research Foundation (FAPESP) through grants #2024/01872-6 (L.F.), #2024/14149-0 (A.F), #2023/06505-9 (M.F.), #2023/00335-4 (J.R), and #2017/21004-5 (L.F.). CEPID CBioClima #2021/10639-5, and project 14805 – FINEP 01.22.0179.00 (MARTMA), as well as by the National Council for Scientific and Technological Development (CNPq) through grant #153850/2024-8 and the National Institute of Science and Technology in Nanotechnology for Sustainable Agriculture (MCTI-CNPq - INCTNanoAgro #405924/2022-4 and CAPES-MEC #88887.953443/2024-00). Also, authors would like to thank Biorender platform for providing the tool that facilitated the design of Fig. 1, enhancing the visual appeal of our paper. Also, thanks are extended to the Bioscience Laboratory (LNBio) for generously allowing the authors to conduct the NMR analyses in their facilities, contributing valuable insights to this research.

Data availability

Data will be made available on request.

Appendix A. Supplementary data

Supplementary data to this article can be found online at https://doi.org/10.1016/j.ijbiomac.2025.144181.

References

[1] V.K. Garlapati, A.K. Chandel, S.P.J. Kumar, S. Sharma, S. Sevda, A.P. Ingle, D. Pant, Circular economy aspects of lignin: towards a lignocellulose biorefinery, Renew. Sustain. Energy Rev. 130 (2020) 109977, https://doi.org/10.1016/j.rser.2020.109977.

[2] Z. Luo, Q. Qian, H. Sun, Q. Wei, J. Zhou, K. Wang, Lignin-first biorefinery for converting lignocellulosic biomass into fuels and chemicals, Energies 16 (2023), https://doi.org/10.3390/en16010125.

[3] N. Akiba, A.T. Omori, I. Gaubeur, Kraft lignin and its derivates – a study on the adsorption of mono and multielement metals, potential use for noble metal recycling and an alternative material for solid base catalyst, Chemosphere 308 (2022) 136538, https://doi.org/10.1016/j.chemosphere.2022.136538.

[4] D.S. Bajwa, G. Pourhashem, A.H. Ullah, S.G. Bajwa, A concise review of current lignin production, applications, products and their environment impact, Ind. Crops Prod. 139 (2019) 111526, https://doi.org/10.1016/j.indcrop.2019.111526.

[5] X. Wang, W. Leng, R.M.O. Nayanathara, D. Milsted, T.L. Eberhardt, Z. Zhang, X. Zhang, Recent advances in transforming agricultural biorefinery lignins into value-added products, J. Agric. Food Res. 12 (2023) 100545, https://doi.org/10.1016/j.jafr.2023.100545.

[6] M.Y. Balakshin, E.A. Capanema, I. Sulaeva, P. Schlee, Z. Huang, M. Feng, M. Borghei, O.J. Rojas, A. Potthast, T. Rosenau, New opportunities in the valorization of technical lignins, ChemSusChem 14 (2021) 1016–1036, https://doi.org/10.1002/cssc.202002553.

[7] J.S. Rodrigues, V. Lima, L.C.P. Araújo, V.R. Botaro, Lignin fractionation methods: can lignin fractions be separated in a true industrial process? Ind. Eng. Chem. Res. 60 (2021) 10863–10881, https://doi.org/10.1021/acs.iecr.1c01704.

[8] H. Sadeghifar, H. Sadeghifar, A. Ragauskas, A. Ragauskas, A. Ragauskas, A. Ragauskas, Perspective on technical lignin fractionation, ACS Sustain. Chem. Eng. 8 (2020) 8086–8101, https://doi.org/10.1021/acssuschemeng.0c01348.

[9] M.J. John, M.C. Lefatle, B. Sithole, Lignin fractionation and conversion to bio-based functional products, Sustain. Chem. Pharm. 25 (2022) 100594, https://doi.org/10.1016/j.scp.2021.100594.

[10] G. Wang, H. Chen, Fractionation of alkali-extracted lignin from steam-exploded stalk by gradient acid precipitation, Sep. Purif. Technol. 105 (2013) 98–105, https://doi.org/10.1016/j.seppur.2012.12.009.

[11] S. Al Arni, Extraction and isolation methods for lignin separation from sugarcane bagasse: a review, Ind. Crop. Prod. 115 (2018) 330–339, https://doi.org/10.1016/j.indcrop.2018.02.012.

[12] T.V. Lourençon, F.A. Hansel, T.A. Da Silva, L.P. Ramos, G.I.B. De Muniz, W.L.E. Magalhães, Hardwood and softwood Kraft lignins fractionation by simple sequential acid precipitation, Sep. Purif. Technol. 154 (2015) 82–88, https://doi.org/10.1016/j.seppur.2015.09.015.

[13] P. Jiang, Q. Li, C. Gao, J. Lu, Y. Cheng, S. Zhai, Q. An, H. Wang, Fractionation of alkali lignin by organic solvents for biodegradable microsphere through self-assembly, Bioresour. Technol. 289 (2019) 121640, https://doi.org/10.1016/j.biortech.2019.121640.

[14] S.Y. Park, J.Y. Kim, H.J. Youn, J.W. Choi, Fractionation of lignin macromolecules by sequential organic solvents systems and their characterization for further valuable applications, Int. J. Biol. Macromol. 106 (2018) 793–802, https://doi.org/10.1016/j.ijbiomac.2017.08.069.

[15] L.C.P. Araújo, F.M. Yamaji, V.H. Lima, V.R. Botaro, Kraft lignin fractionation by organic solvents: correlation between molar mass and higher heating value, Bioresour. Technol. 314 (2020) 123757, https://doi.org/10.1016/j.biortech.2020.123757.

[16] N. Kumar, S. Vijayshankar, P. Pasupathi, Optimal extraction , sequential fractionation and structural characterization of soda lignin, Res. Chem. Intermed. 44 (9) (2018) 5403–5417, https://doi.org/10.1007/s11164-018-3430-0.

[17] S. Aminzadeh, M. Lauberts, G. Dobele, J. Ponomarenko, T. Mattsson, M.E. Lindström, O. Sevastyanova, Membrane filtration of Kraft lignin: structural charactristics and antioxidant activity of the low-molecular-weight fraction, Ind. Crops Prod. 112 (2018) 200–209, https://doi.org/10.1016/j.indcrop.2017.11.042.

[18] A.S. Jönsson, A.K. Nordin, O. Wallberg, Concentration and purification of lignin in hardwood Kraft pulping liquor by ultrafiltration and nanofiltration, Chem. Eng. Res. Des. 86 (2008) 1271–1280, https://doi.org/10.1016/j.cherd.2008.06.003.

[19] J. Fernández-Rodríguez, X. Erdocia, F. Hernández-Ramos, M.G. Alriols, J. Labid, Lignin separation and fractionation by ultrafiltration, in: Sep. Funct. Mol. Food by Membr. Technol., 2018, pp. 229–265, https://doi.org/10.1016/B978-0-12-815056-6.00007-3.

[20] G. Tofani, E. Jasiukaitytė-Grojzdek, M. Grilc, B. Likozar, Organosolv biorefinery: resource-based process optimisation, pilot technology scale-up and economics, Green Chem. 26 (2023) 186–201, https://doi.org/10.1039/d3gc03274d.

[21] J.A. Ferreira, M.J. Taherzadeh, Improving the economy of lignocellulose-based biorefineries with organosolv pretreatment, Bioresour. Technol. 299 (2020) 122695, https://doi.org/10.1016/j.biortech.2019.122695.

[22] V.R. Botaro, J.S. Rodrigues, A Desconstrução Dos Tecidos Vegetais E Possibilidades Atuais de produção de Novos Materiais, 1st ed., Editora Espaço Acadêmico, Goiânia, 2019. http://www.ppgcm.ufscar.br/arquivos/adesconstrucao_ebook16_12.pdf.

[23] D.R. de Oliveira, F. Avelino, S.E. Mazzetto, D. Lomonaco, Microwave-assisted selective acetylation of Kraft lignin: acetic acid as a sustainable reactant for lignin valorization, Int. J. Biol. Macromol. 164 (2020) 1536–1544, https://doi.org/10.1016/j.ijbiomac.2020.07.216.

[24] J.S. Rodrigues de, A.S.M. Freitas, C.C. Maciel, S.F. Mendes, D. Diment, M. Balakshin, V.R. Botaro, Selection of kraft lignin fractions as a partial substitute for phenol in synthesis of phenolic resins: structure-property correlation, Ind. Crops Prod. 191 (2023) 115948, https://doi.org/10.1016/j.indcrop.2022.115948.

[25] M. Morsali, A. Moreno, A. Loukovitou, I. Pylypchuk, M.H. Sipponen, Stabilized lignin nanoparticles for versatile hybrid and functional nanomaterials, Biomacromolecules (2022), https://doi.org/10.1021/acs.biomac.2c00840.

[26] M. Balakshin, E. Capanema, On the quantification of lignin hydroxyl groups with 31P and 13C NMR spectroscopy, J. Wood Chem. Technol. 35 (2015) 220–237, https://doi.org/10.1080/02773813.2014.928328.

[27] T. Swain, W.E. Hillis, The phenolic constituents of Prunus domestica. I.—the quantitative analysis of phenolic constituents, J. Sci. Food Agric. 10 (1959) 63–68, https://doi.org/10.1002/jsfa.2740100110.

[28] W. Brand-Williams, M.E. Cuvelier, C. Berset, Use of a free radical method to evaluate antioxidant activity, LWT - Food Sci. Technol. 28 (1995) 25–30, https://doi.org/10.1016/S0023-6438(95)80008-5.

[29] L. Xu, J. Zhang, Q.J. Zong, L. Wang, T. Xu, J. Gong, Z.H. Liu, B.Z. Li, Y.J. Yuan, High-solid ethylenediamine pretreatment to fractionate new lignin streams from lignocellulosic biomass, Chem. Eng. J. 427 (2022), https://doi.org/10.1016/j.cej.2021.130962.

[30] F. Antunes, I.F. Mota, J. da Silva Burgal, M. Pintado, P.S. Costa, A review on the valorization of lignin from sugarcane by-products: from extraction to application, Biomass Bioenergy 166 (2022), https://doi.org/10.1016/j.biombioe.2022.106603.

[31] F.G.C. Pinheiro, A.K.L. Soares, S.T. Santaella, L.M.A.e. Silva, K.M. Canuto, C.A. Cáceres, M. de F. Rosa, J.P. de A. Feitosa, R.C. Leitão, Optimization of the acetosolv extraction of lignin from sugarcane bagasse for phenolic resin production, Ind. Crops Prod. 96 (2017) 80–90, https://doi.org/10.1016/j.indcrop.2016.11.029.

[32] I. de Menezes Nogueira, F. Avelino, D.R. de Oliveira, N.F. Souza, M.F. Rosa, S.E. Mazzetto, D. Lomonaco, Organic solvent fractionation of acetosolv palm oil lignin: the role of its structure on the antioxidant activity, Int. J. Biol. Macromol. 122 (2019) 1163–1172, https://doi.org/10.1016/j.ijbiomac.2018.09.066.

[33] M. Arefmanesh, S. Nikafshar, E.R. Master, M. Nejad, From acetone fractionation to lignin-based phenolic and polyurethane resins, Ind. Crops Prod. 178 (2022) 114604, https://doi.org/10.1016/j.indcrop.2022.114604.

[34] Y. Zhang, M. Jiang, Y. Zhang, Q. Cao, X. Wang, Y. Han, G. Sun, Y. Li, J. Zhou, Novel lignin–chitosan–PVA composite hydrogel for wound dressing, Mater. Sci. Eng. C 104 (2019) 110002, https://doi.org/10.1016/j.msec.2019.110002.

[35] N. Giummarella, P.A. Lindén, D. Areskogh, M. Lawoko, Fractional profiling of Kraft lignin structure: unravelling insights on lignin reaction mechanisms, ACS Sustain. Chem. Eng. 8 (2020) 1112–1120, https://doi.org/10.1021/acssuschemeng.9b06027.

[36] E. Melro, A. Filipe, D. Sousa, A.J.M. Valente, A. Romano, F.E. Antunes, B. Medronho, Dissolution of Kraft lignin in alkaline solutions, Int. J. Biol. Macromol. 148 (2020) 688–695, https://doi.org/10.1016/j.ijbiomac.2020.01.153.

[37] A. Dastpak, T.V. Lourençon, M. Balakshin, S. Farhan Hashmi, M. Lundström, B.P. Wilson, Solubility study of lignin in industrial organic solvents and investigation of electrochemical properties of spray-coated solutions, Ind. Crops Prod. 148 (2020) 112310, https://doi.org/10.1016/j.indcrop.2020.112310.

[38] J. Singh, A.S. Dhaliwal, Electrochemical and photocatalytic degradation of methylene blue by using rGO/AgNWs nanocomposite synthesized by electroplating on stainless steel, J. Phys. Chem. Solid 160 (2022) 110358, https://doi.org/10.1016/j.jpcs.2021.110358.

[39] P. Manara, A. Zabaniotou, C. Vanderghem, A. Richel, Lignin extraction from Mediterranean agro-wastes: impact of pretreatment conditions on lignin chemical structure and thermal degradation behavior, Catal. Today 223 (2014) 25–34, https://doi.org/10.1016/j.cattod.2013.10.065.

[40] M. El Moustaqim, A. El Kaihal, M. El Marouani, S. Men-la-yakhaf, Thermal and thermomechanical analyses of lignin, Sustain. Chem. Pharm. 9 (2018) 63–68, https://doi.org/10.1016/j.scp.2018.06.002.

[41] C. Gao, L. Zhou, S. Yao, C. Qin, P. Fatehi, Phosphorylated Kraft lignin with improved thermal stability, Int. J. Biol. Macromol. 162 (2020) 1642–1652, https://doi.org/10.1016/j.ijbiomac.2020.08.088.

[42] P. Mousavioun, W.O.S. Doherty, Chemical and thermal properties of fractionated bagasse soda lignin, Ind. Crops Prod. 31 (2010) 52–58, https://doi.org/10.1016/j.indcrop.2009.09.001.

[44] J. Rumpf, R. Burger, M. Schulze, Statistical evaluation of DPPH, ABTS, FRAP, and Folin-Ciocalteu assays to assess the antioxidant capacity of lignins, Int. J. Biol. Macromol. 233 (2023), https://doi.org/10.1016/j.ijbiomac.2023.123470.

[45] Y. Li, M. Chen, Q.S. Shi, X. Xie, Y. Guo, Biomass fractionation techniques impact on the structure and antioxidant properties of isolated lignins, Sep. Purif. Technol. 330 (2024) 125499, https://doi.org/10.1016/j.seppur.2023.125499.

[46] Z. Mahmood, M. Yameen, M. Jahageer, M. Raiz, A. Graffar, I. Javid, Lignin as natural antioxidant capacity, in: Lignin - Trends Appl., 2018, pp. 1–27 (https://www.intechopen.com/books/advanced-biometric-technologies/liveness-detection-in-biometrics).

[47] L. Matsakas, M. Gerber, L. Yu, U. Rova, P. Christakopoulos, Preparation of low carbon impact lignin nanoparticles with controllable size by using different strategies for particles recovery, Ind. Crops Prod. 147 (2020) 112243, https://doi.org/10.1016/j.indcrop.2020.112243.

[48] I.V. Pylypchuk, A. Riazanova, M.E. Lindström, O. Sevastyanova, Structural and molecular-weight-dependency in the formation of lignin nanoparticles from fractionated soft- and hardwood lignins, Green Chem. 23 (2021) 3061–3072, https://doi.org/10.1039/d0gc04058d.

[49] C. Frangville, M. Rutkevičius, A.P. Richter, O.D. Velev, S.D. Stoyanov, V.N. Paunov, Fabrication of environmentally biodegradable lignin nanoparticles, ChemPhysChem 13 (2012) 4235–4243, https://doi.org/10.1002/cphc.201200537.

[50] L. Matsakas, A. Karnaouri, A. Cwirzen, U. Rova, P. Christakopoulos, Formation of lignin nanoparticles by combining organosolv pretreatment of birch biomass and homogenization processes, Molecules 23 (2018), https://doi.org/10.3390/molecules23071822.

[51] S. Bhatnagar, T. Kobori, D. Ganesh, K. Ogawa, H. Aoyagi, Biosynthesis of silver nanoparticles mediated by extracellular pigment from talaromyces purpurogenus and their biomedical applications, Nanomaterials 9 (2019), https://doi.org/10.3390/nano9071042.

[52] X. Zhang, M. Tu, M.G. Paice, Routes to potential bioproducts from lignocellulosic biomass lignin and hemicelluloses, Bioenergy Res. 4 (2011) 246–257, https://doi.org/10.1007/s12155-011-9147-1.

[53] M.Y. Chan, Q.M. Dowling, S.J. Sivananthan, R.M. Kramer, Particle sizing of nanoparticle adjuvant formulations by dynamic light scattering (DLS) and nanoparticle tracking analysis (NTA), Methods Mol. Biol. 1494 (2017) 239–252, https://doi.org/10.1007/978-1-4939-6445-1_17.

[54] W. Zhao, L.P. Xiao, G. Song, R.C. Sun, L. He, S. Singh, B.A. Simmons, G. Cheng, From lignin subunits to aggregates: insights into lignin solubilization, Green Chem. 19 (2017) 3272–3281, https://doi.org/10.1039/c7gc00944e.

[55] M. Österberg, M.H. Sipponen, B.D. Mattos, O.J. Rojas, Spherical lignin particles: a review on their sustainability and applications, Green Chem. 22 (2020) 2712–2733, https://doi.org/10.1039/d0gc00096e.

[56] M. Lievonen, J.J. Valle-Delgado, M.L. Mattinen, E.L. Hult, K. Lintinen, M.A. Kostiainen, A. Paananen, G.R. Szilvay, H. Setälä, M. Österberg, A simple process for

lignin nanoparticle preparation, Green Chem. 18 (2016) 1416–1422, https://doi.org/10.1039/c5gc01436k.
[57] A. do E.S. Pereira, J. Luiz de Oliveira, S. Maira Savassa, C. Barbara Rogério, G. Araujo de Meiros, L.F. Fraceto, Lignin nanoparticles: new insights for a sustainable agriculture, J. Clean. Prod. 345 (2022) 131145, https://doi.org/10.1016/j.jclepro.2022.131145.
[58] S.R. Yearla, K. Padmasree, Preparation and characterisation of lignin nanoparticles: evaluation of their potential as antioxidants and UV protectants, J. Exp. Nanosci. 11 (2016) 289–302, https://doi.org/10.1080/17458080.2015.1055842.
[59] J. Tomasich, S. Beisl, M. Harasek, Production and characterisation of pickering emulsions stabilised by colloidal lignin particles produced from various bulk lignins, Sustain 15 (4) (2023) 3693, https://doi.org/10.3390/su15043693.
[60] J.S. Rodrigues, A.S.M. de Freitas, H.O.S. Vieira, L.S. Emidio, S.F. Amaro, M.A. Azevedo, I.C.S. Duarte, V.R. Botaro, L.F. Fraceto, M. Ferreira, Designing sustainable soil conditioners: nanocomposite-based thermoplastic starch for enhanced soil health and crop performance, Int. J. Biol. Macromol. 297 (2025), https://doi.org/10.1016/j.ijbiomac.2025.139747.